IEEE Access
Multidisciplinary | Rapid Review | Open Access Journal

Received 1 July 2022, accepted 25 July 2022, date of publication 29 July 2022, date of current version 4 August 2022.

Digital Object Identifier 10.1109/ACCESS.2022.3195029

RESEARCH ARTICLE

Bloodstain Identification Based on Visible/Near-Infrared Hyperspectral Imaging With Convolutional Neural Network

YUNAN HE[1], CHENXUAN YANG[1], SHENG JIANG[1], ZHIJI DENG[2], PENG ZHAO[1], AND YE LI[1]

[1]School of Physics, Electronic Science and Technology, Changchun University of Science and Technology, Changchun 130022, China
[2]Zhejiang Dahua Technology Company Ltd., Hangzhou 310053, China

Corresponding authors: Ye Li (liyecust@163.com) and Peng Zhao (zp123890@163.com)

ABSTRACT Blood samples are easily damaged in traditional bloodstain detection and identification. In complex scenes with interfering objects, bloodstain identification may be inaccurate, with low detection rates and false-positive results. In order to meet these challenges, we propose a bloodstain detection and identification method based on hyperspectral imaging and mixed convolutional neural networks, which enables fast and efficient non-destructive identification of bloodstains. In this study, we apply visible/near-infrared reflectance hyperspectral imaging in the 380-1000 nm spectral region to analyze the shape, structure, and biochemical characteristics of bloodstains. Hyperspectral images of bloodstains on different substrates and six bloodstain analogs are experimentally obtained. The acquired spectral pixels are pre-processed by Principal Component Analysis (PCA). For bloodstains and different bloodstain analogs, regions of interest are selected from each substance to obtain pixels, which are further used in convolutional neural network (CNN) modeling. After the mixed CNN modeling is completed, pixels are selected from the hyperspectral images as a test set for bloodstains and bloodstain analogs. Finally, the bloodstain recognition ability of the mixed 2D-3D CNN model is evaluated by analyzing the kappa coefficient and classification accuracy. The experimental results show that the accuracy of the constructed CNN bloodstain identification model reaches 95.4%. Compared with other methods, the bloodstain identification method proposed in this study has higher efficiency and accuracy in complex scenes. The results of this study will provide a reference for the future development of the bloodstain online detection system.

INDEX TERMS Bloodstain identification, visible/near-infrared, hyperspectral imaging, deep learning, convolutional neural networks, feature extraction.

I. INTRODUCTION

Blood is one of the most common liquids found at violent crime scenes, and investigators generally need to examine blood to determine the relationship between a victim and a suspects in a criminal case. However, bloodstain detection need to meet certain requirements, including the external and internal characteristics of bloodstains (e.g., color, location, authenticity, etc.). Moisture content and hemoglobin in blood are two important intrinsic factors that determine the nature of bloodstains. At present, most bloodstain detection techniques employ destructive methods. In some specific scenarios, bloodstains may be wiped or cleaned, resulting in scarcity of blood samples. The use of destructive detection methods will undoubtedly make it difficult to conduct other tests in the future. Therefore, a detection method is needed that is fast, reliable, and shows the characteristics of bloodstains in all aspects in a non-destructive way. To this purpose, we propose a visual detection method that combines hyperspectral imaging techniques with convolutional neural networks to improve the ability to detect the physical features such as the size, shape, location, and relationship to the substrate of bloodstain patterns [1].

In recent years, hyperspectral imaging, as a fast, reliable, and non-destructive analysis technique, has been widely concerned and applied in various fields. It can be used

The associate editor coordinating the review of this manuscript and approving it for publication was Gustavo Callico.

to detect the internal properties of food products [2]–[4], analyze the chemical composition of pharmaceuticals [5], [6], do medical research [7], [8], and do some non-destructive testing [9], [10], etc. Hyperspectral imaging is a technique that combines image information with spectral information to record spectral information in different wavelength ranges. In addition, it allows the simultaneous qualitative and quantitative analysis of the intrinsic chemical properties, physical properties, and spatial distribution of bloodstain samples. With this technique, researchers can understand the interactions between photons and molecules in a scene of specific wavelengths [11]. If we analyze the spectral profiles and spectral images further, we can use this interaction to determine the presence of target bloodstains or other substances at the scene.

Although visible/near-infrared hyperspectral imaging has many advantages, more useful information can be obtained and provided than other multispectral techniques. However, hyperspectral imaging still faces enormous challenges, such as the huge amount of information that can cause problems in data processing [12]. The main problems of hyperspectral data processing are manifested in the dimensionality problems caused by a large number of channels, and the variation of spatial dimension can cause data sparsity and other troubles. At the same time, the precise spectral resolution also brings a large amount of redundant data, which requires a reduction in the dimension of spectral data [13]. However, the spatial nature of spectral data is very complex, and it is not easy to reduce the dimension while ensuring sufficient spectral data information. On the other hand, the use of hyperspectral imaging to design an accurate and efficient detection scheme is also a major challenge.

Currently, with the continuous development of deep learning, researchers have introduced many new methods in the field of hyperspectral image classification, such as support vector machines (SVM) [14], CNN [15], etc. Compared with the more complex and difficult to implement traditional algorithms, the neural network-based method can well overcome the problems caused by the complexity of calculation in the case of multi-classification. CNN is a representative and highly effective deep learning method. It simulates the process of neuron processing problems in the human brain through a hierarchy of input layer, hidden layer, fully connected layer, and output layer. The design of an effective CNN model avoids artificial feature extraction and conduct in-depth learning of features at different levels. Ding *et al.* proposed a method of semi-supervised locality preserving dense graph neural network with ARMA filters and context-aware learning for hyperspectral image classification [16], which greatly reduces the computational cost and can effectively suppress noise. Ding *et al.* proposed a method of graph sample and aggregate-attention network for hyperspectral image classification [17], which can automatically learn the deep background and global information by using an attention mechanism to characterize the importance between spatially adjacent regions. Ding *et al.* proposed the method of multiscale graph sample and aggregate network with context-aware learning for hyperspectral image classification [18]. By learning multi-scale features from local regions, the diversity of network input information can be improved and the impact of inputting wrong original images on classification can be effectively addressed. Huang *et al.* used a one-dimensional convolutional neural network (1D-CNN) to classify bloodstains in the spectral domain [19]. Although deep learning performs well in a variety of visualization tasks in image classification, training datasets is still required to achieve higher accuracy.

At present, there are few studies on blood classification using deep learning methods, and detection tasks in complex environments will be more complicated to perform. To this end, this study proposes a mixed network model based on 2D-CNN and 3D-CNN, and compares it with 1D-CNN [20], 2D-CNN [21], and 3D-CNN [22] to better identify hyperspectral bloodstain data.

The main contributions of this study are shown as follows:

(1) A new method for detecting bloodstain using hyperspectral imaging is proposed. By designing a mixed convolutional neural network(CNN), we can accurately detect bloodstains and bloodstain analogs on complex scenes and different substrates.

(2) Due to the large amount of spectral data, we have designed a targeted method to reduce the redundancy of spectral data. This method can retain useful spectral data information while removing a large amount of repetitive or irrelevant spectral information.

(3) A bloodstain spectral information detection model is constructed. This model accurately distinguishes between bloodstains, artificial blood, ketchup and many other bloodstain analogs. The detection rate remains very reliable for complex scenes and substrates. Compared with other state-of-the-art methods, the model proposed in this study has more advantages in terms of detection efficiency and identification accuracy.

The rest of this article is divided into four parts. The first part introduces the data content as well as data processing and modeling methods. The second part is a demonstration of results. The third part discusses and analyzes the experimental results. The last part is a conclusion and a description of possible future work.

II. MATERIALS AND METHODS

A. HYPERSPECTRAL IMAGING SYSTEM

A push-scan hyperspectral camera (Headwall Photonics, Resonon, Inc., RA1000m/D_DFG) is used in this study. The whole system consists of four parts in total: a Headwall hyperspectral camera, a hyperspectral illumination circuit, a motorized positioning sample stage driven by stepper motors, and a computer (i7-7700HQ CPU). The composed hyperspectral imaging system is shown in Figure 1. To avoid interference of stray light to the experiment, the system is placed in a dark room without stray light. On the other

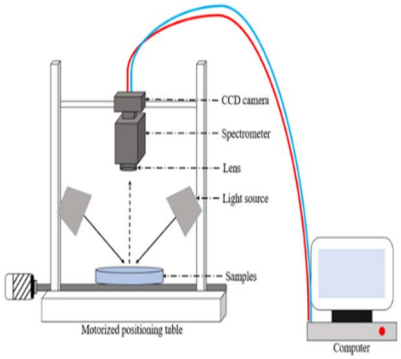

FIGURE 1. Schematic diagram of the hyperspectral imaging system.

hand, the experiment requires setting up the equipment acquisition parameters in advance to obtain visible/near-infrared hyperspectral images as soon as possible. This is done to avoid the thermal effect of the light source on the experiment and to obtain a higher-quality image. In this study, the distance between the camera and the sample is adjusted to 40 cm, and the illumination source is set at an angle of 45° to the horizontal plane. The movement speed of the mechanical stage is set to 20 mm/s, and the camera exposure time is set to 1 ms. The whole system acquires spectral images in the wavelength range of 380-1000 nm with a spectral resolution of 4.84 nm. For the acquired visible/near-infrared hyperspectral images, each image contains 128 single wavelengths in the full spectral range. The presence of dark currents in the camera itself causes a lot of noise in some bands with low light intensity. Therefore, before further experiments, the acquired hyperspectral images need to be corrected with white reference (RW) and black reference (RB). The correction method is to use a white diffuse reflectance plate with 99% reflectance efficiency to acquire a white reference image. The black reference image with 0% reflectance is acquired by covering the lens cap in a light-free environment.

B. EXPERIMENTAL SAMPLE

The experimental samples used in this study were designed by our laboratory and the blood samples were provided by three volunteers. Several different target detection scenes were set up for this study. This included background materials of different colors and compositions, as well as different experimental samples. Bloodstains of different sizes and shapes were placed on the substrate as well as substances that were visually similar to the bloodstains, such as ketchup, artificial blood, oil-soluble pigment, beetroot juice, acrylic paint, and sweet-spicy sauce. Due to their similarity in color, it is difficult to discern them with the naked eye in certain special cases. Therefore, our experiment intends to solve this problem using hyperspectral images combined with a convolutional diviner network.

Figure 2 illustrates a standard experimental scene, this scenario simulates a bloodstain identification exercise in a laboratory setting with bloodstains as well as six bloodstain

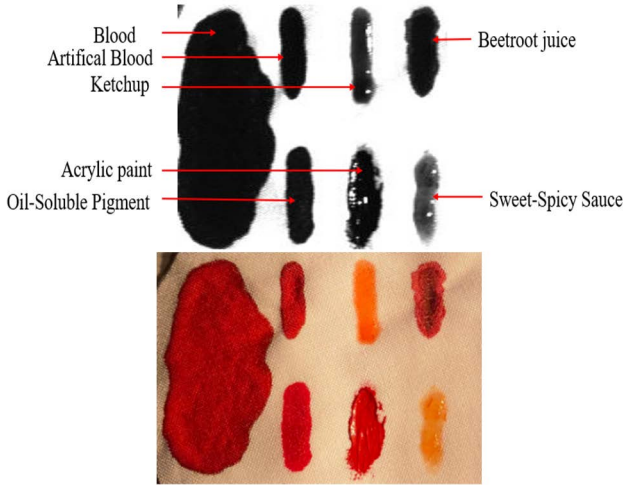

FIGURE 2. Standard bloodstain detection model under laboratory.

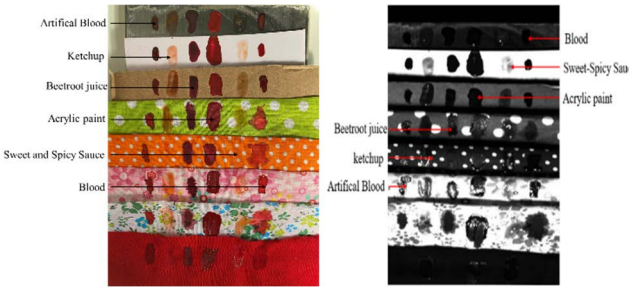

FIGURE 3. Hyperspectral images of bloodstains in complex scenes.

analogs on a white fabric substrate. This set of blood spectral data was obtained as an experiment by taking multiple shots at different times.

Figure 3 shows a more complex scene with bloodstain and five bloodstain analogs in eight different material backgrounds. The background complexity and environmental diversity of this scene make the detection task more challenging.

C. SPECTRAL DATA EXTRACTION AND PRETREATMENT

The hyperspectral data used in this study contains 128 bands, and such a huge amount of data will cause difficulties for subsequent data processing. To remove the spectral redundant data, this study adopts the method of Principal Component Analysis (PCA) to do dimensionality reduction on the raw hyperspectral data for the spectral bands.

Feature extraction is to find the optimal solution in the process of visualization and machine learning. In this study, PCA [23] is used to reduce the dimensionality of the data. We map 128-dimensional features to 3 dimensions, and ignore very similar detailed information. The PCA transformation formula is as follows:

$$P = W \times S \tag{1}$$

In formula (1), S is the initial data set, W is the transformation matrix, and P is the obtained dimensionality reduction data. The transformation matrix is obtained according to the

following formula:

$$(\lambda I - C)\mathrm{E} = 0\lambda \tag{2}$$

where C is the covariance matrix of S, I is the unit matrix, E is the eigenvector of C, and λ is the eigenvalue matrix of C. The eigenvector E is expressed as:

$$\mathrm{E} = [a_1, a_2, a_3, \ldots a_n] \tag{3}$$

where a satisfies the following equation:

$$aa^T = a^T a = 1 \tag{4}$$

The transformation matrix W consists of several a^T corresponding to the largest eigenvalues, and the sum of the eigenvalues is 95% of C.

Finally, the non-negative matrix decomposition (NMF) is used to reduce the dimensionality of the non-negative data matrix, and the principle is as follows:

$$V \approx W \times H \tag{5}$$

where V denotes the original matrix, and W and H represent the smaller matrices into which it is decomposed. By this principle and performing several iterations, the original input matrix is decomposed into a weight matrix and an eigenmatrix to achieve data dimensionality reduction.

D. ESTABLISHMENT OF MODELS

At present, most classification models use 2D-CNN or 3D-CNN for feature extraction. Among them, 2D-CNN is a classical deep learning algorithm, which has performed well in machine vision tasks such as image classification and target detection [24], [25]. 2D-CNN has the advantage that features can be extracted directly from images, which is end-to-end processing. The equation of the convolution process is as follows:

$$V_{1j}^{xy} = f\left(\sum_m \sum_{h=0}^{H_{I-1}} \sum_{w=0}^{W_{I-1}} K_{1jm}^{hw} V_{(I-1)m}^{(x+h)(y+w)} + b_{1j}\right) \tag{6}$$

where m is the number of channels, H_{I-1} and W_{I-1} are the convolution kernel sizes, and K and b are linear coefficients.

When 2D convolutional processing, each channel needs to train convolutional kernels. While the number of channels in hyperspectral images is large, if 2D-CNN is directly used to process hyperspectral image data, it will lead to a large introduction of parameters, which will reduce the training efficiency and speed of the network, and more likely affect the final accuracy.

Compared with 2D-CNN, 3D-CNN has the advantage of one more convolutional kernel R_{I-1}, which makes it well compensate for the shortcomings of 2D-CNN. Its convolutional model equation is described as follows:

$$V_{1j}^{xyz} = f\left(\sum_m \sum_{h=0}^{H_{I-1}} \sum_{w=0}^{W_{I-1}} \sum_{r=0}^{R_{I-1}} K_{1jm}^{hwr} V_{(I-1)m}^{(x+h)(y+w)(z+r)} + b_{1j}\right) \tag{7}$$

However, the deepening of the network has also brought about problems such as gradient explosion and longer calculation time, and if the training data is limited, over-fitting may also occur.

Since hyperspectral images are stereoscopic data and contain massive information, 1D-CNN or 2D-CNN cannot extract the feature information of the target object from the spectral dimension well. 3D-CNN kernel can extract spatial and spectral information from hyperspectral images, but the cost is that the parameters of the network are too large, which increases the computational complexity and makes the model difficult to be applied in practice.

In order to alleviate the above problems, in this study, we propose a mixed CNN model framework that combines 2D-CNN and 3D-CNN, as shown in Figure 4. The model includes 3D-convolution, 2D-convolution and fully-connected layers, and after the features are extracted in different convolutional layers, the data are fed into the fully-connected layer for classification and then output. The model can make full use of the spectral information and spatial feature maps of bloodstains, and retains the spatial-temporal feature based on 2D-CNN to achieve the maximum possible accuracy of bloodstain detection.

The dimensions of the 3D convolutional kernels of the proposed mixed model are: conv1 is 8 convolutional kernels of $7 \times 7 \times 3$; conv2 is 16 convolutional kernels of $5 \times 3 \times 3$; and conv3 is 32 convolutional kernels of $3 \times 3 \times 3$. The dimensionality of the 2D convolutional kernels is: conv4 is 64 convolutional kernels of $3 \times 3 \times 3$, which is done because small $3 \times 3 \times 3$ convolutional kernels are the best choice for input spatial-temporal feature learning. Also, the processing method using one two-dimensional convolution can distinguish the spatial information of different spectral bands without losing spectral information. This inspiration comes from the processing of some 3D medical CT images, because both hyperspectral and CT images have image information as well as similar 3D data.

The 2D convolutional layers are placed after successive 3D convolutional layers to further differentiate the features. To adapt to the input dimension of the 2D convolutional layer, the feature cube generated by the 3D convolutional layer is connected to the spectral dimension, i.e. the dimension $\mathrm{W} \times \mathrm{H} \times \mathrm{B} \times \mathrm{C}$ of the four-dimensional tensor is reshaped into $\mathrm{W} \times \mathrm{H} \times \mathrm{BC}$. The traditional 2D convolution is then replaced with a deeply separable convolution, which can improve usage efficiency, simplify network training, and enhance spectral information flow in the network.

As can be seen from the traditional 2D convolution process, in terms of feature map generation, spatial dimensions and channel information are mapped simultaneously. Unlike traditional 2D convolution, we first convolve each channel of the input data with 2D convolution kernels, setting the number of kernels to 1 for deep convolution. The second step is similar to the traditional 2D convolution with a kernel size of 1×1. This is shown in Figure 5. Compared to traditional 2D convolution, this method reduces the possibility of

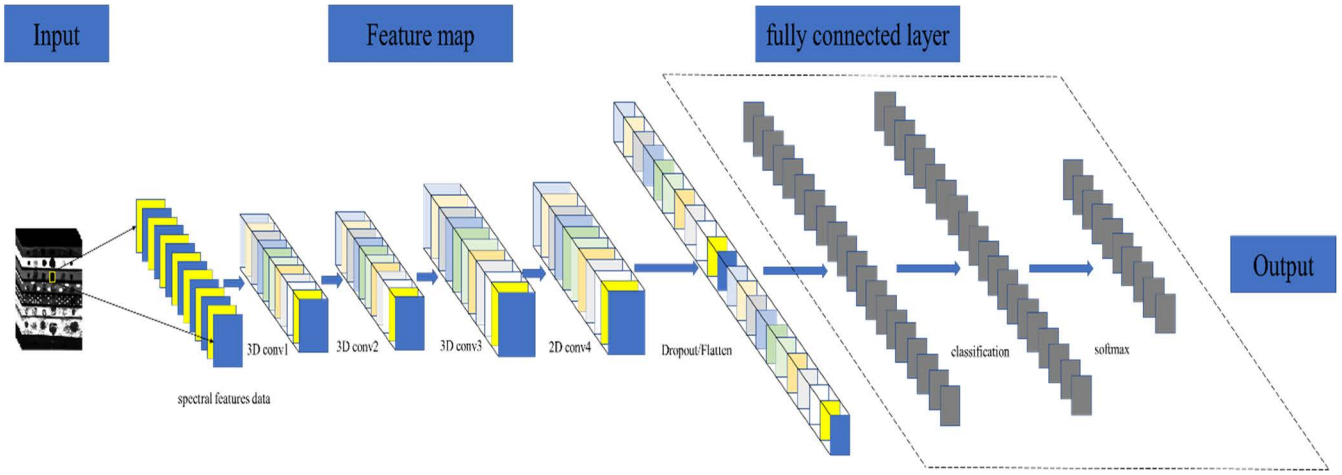

FIGURE 4. Schematic diagram of the structure of the bloodstain recognition model based on mixed 2D-3D CNN.

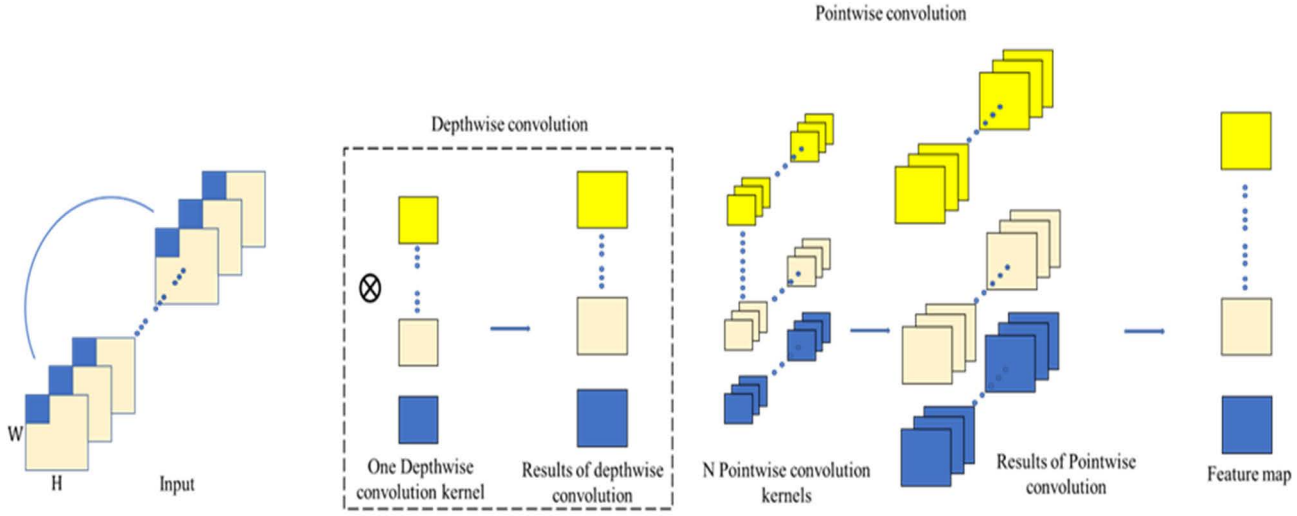

FIGURE 5. Deeply separable convolution operation.

overfitting in the classification task. On the other hand, the training speed of the network is accelerated.

The application of deeply separable convolution can improve spectral classification performance. The main advantage is the reduction in the number of parameters and the number of calculations. Secondly, the cascaded feature maps generated from successive 3D convolution layers can contain extremely informative spectral information in the neighborhood of the pixel to be classified.

E. DATA PROCESSING

Anaconda3-5.2.0, MATLAB 2018b, Excel 2019 (Microsoft, USA) software is used for data processing in this study. Hyperspectral images of bloodstains and blood analogs in two scenes are firstly obtained by acquisition. Secondly, dark current correction and whiteboard correction are performed. The third step is to extract the spectral information of the bloodstains and bloodstain analogs, and the huge spectral data are processed by dimensionality reduction to remove redundant information. Then, the pixel data of the labeled regions are used to build a CNN model. And the remaining labeled sample pixel regions are used as the test set. The specific processing flow of the experiment is shown in Figure 6. The wavelengths from 380-1000 nm (a total of 128 bands) are analyzed experimentally.

III. EXPERIMENT RESULTS AND DISCUSSION

A. HYPERSPECTRAL IMAGING SYSTEM

This section shows the results of the experiments, and the results are compared and discussed. In this study, our proposed method has been implemented in Anaconda 3-5.2.0 software and tested on hyperspectral images of bloodstains in a laboratory scene and complex scenes. All experiments were performed on an Intel Core i7-7700HQ

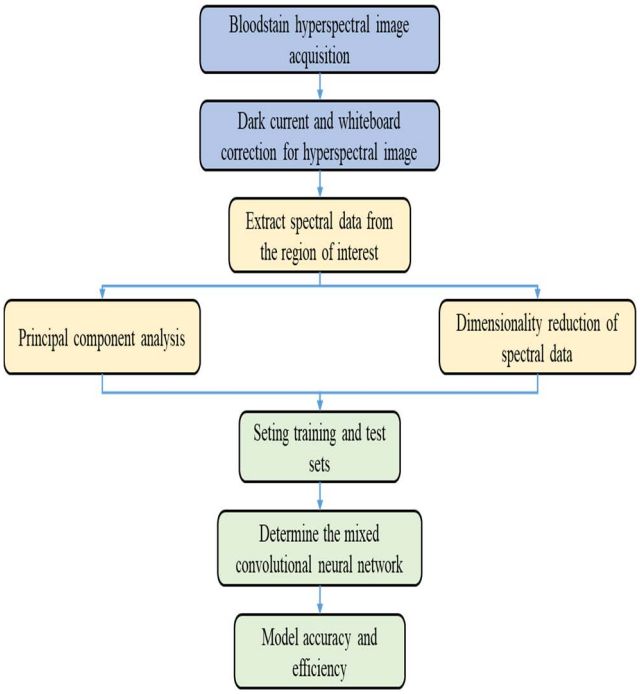

FIGURE 6. Data processing process.

@2.80GHZ 8GB computer and computed by a CUAD GPU device.

To take full advantage of hyperspectral image classification techniques, a cube of HIS data is divided into small overlapping 3D patches with the truth labels determined by the labels of the central pixels. In the network framework of this study, the 3D convolution kernel dimensions are $8 \times 7 \times 7 \times 3$, $16 \times 5 \times 3 \times 3$, and $32 \times 3 \times 3 \times 3$. The 2D convolution kernel has a dimension of $64 \times 3 \times 3$, with 64 representing the number of kernels and 3×3 denoting the spatial dimension of the 2D kernel. Three three-dimensional convolutions are used to increase the number of spectral-spatial feature maps so that the spectral information of the data can then be retained in the output cube. Then two-dimensional convolution is used once because it strongly distinguishes spatial information within different spectral bands and does not result in a loss of spectral information. Table 1 summarizes the layer types, output map dimensions and number of parameters for the proposed model.

B. HYPERSPECTRAL SPECTRAL ANALYSIS

Hemoglobin is the main component for identifying bloodstains is. The main role of hemoglobin in blood is to transport the element oxygen to various organs of the body. Hemoglobin is made up of four hemoglobin subunits, two alpha chains and two beta chains.

The hemoglobin subunit contains a peptide chain and a hematoxylin molecule, and the peptide chain is coiled and folded into a spherical shape, sandwiching the hemoglobin molecule inside. The hemoglobin molecule is a small

TABLE 1. Layer types, output map dimensions, number of parameters for the proposed model.

Layer(type)	Output Shape	Parameter
Conv3d-1	(23,23,28,8)	14592
Conv3d-2	(21,21,18,16)	32896
Conv3d-3	(19,19,24,32)	130304
Reshape	(19,19,256)	0
Conv2d-1	(17,17,256)	16,512
flatten	(73984)	0
dense	(256)	277767
dropout	(256)	0
dense	(128)	18684
dropout	(128)	0
dense	(7)	903

molecule of porphyrin structure, bound at the center of the porphyrin molecule by four nitrogen atoms on a pyrrole ring and a ferrous ion ligand. In an aerobic environment, hemoglobin carries oxygen for movement and oxygen molecules take the place of water molecules, coordinating their binding to ferrous ions. In the internal environment, hemoglobin's main function is to transport oxygen and carbon dioxide to the organs, maintaining the body's normal requirements.

The function of hemoglobin in transporting oxygen determines its presence in the body environment in the form of different derivatives. There are two main forms of hemoglobin in the body: deoxyhemoglobin (Hb) and oxyhemoglobin (HbO2), which is bound to oxygen and is converted by various catalytic enzymes and hormones in the body. In addition, a small amount of HBO2 is oxidized to methemoglobin (Met-Hb). Met-Hb is unable to bind oxygen, but is catalyzed by the action of reductase enzymes to reduce it to HB. Based on the presence of these hemoglobin derivative components in blood, blood shows a complete system of absorption bands in the visible/near-infrared regions of the spectrum. The structure of the absorption spectra of the HB derivatives varies considerably, with strong absorption in the band between 400-425 nm. In the presence of HBO2, two strong absorption peaks are also produced in the 500-600 nm band of the spectrum.

The spectral profile of a substance is a visual representation of its internal components. The bloodstain spectrum is a representation of hemoglobin and its derivatives, and this representation is determined by the specific gravity of the various components in the bloodstain. The spectral profile of a bloodstain can be seen as a specific gravity fit to the spectra of the various components of the substance, which in the internal environment are mainly determined by HB and HBO2. The in vitro environment is also influenced by Met-Hb and hemichromatin.

Overall, the bloodstain spectral profile has three identifiable features in the visible/near-infrared band range, one being a strong absorption peak in the 400-425 nm band. Another is a strong absorption peak in the 500-600 nm band due to the presence of a large amount of HBO2, where the reflectance amplitude is weak and the reflectance spectrum shows a trough. The last identifying feature is the strong

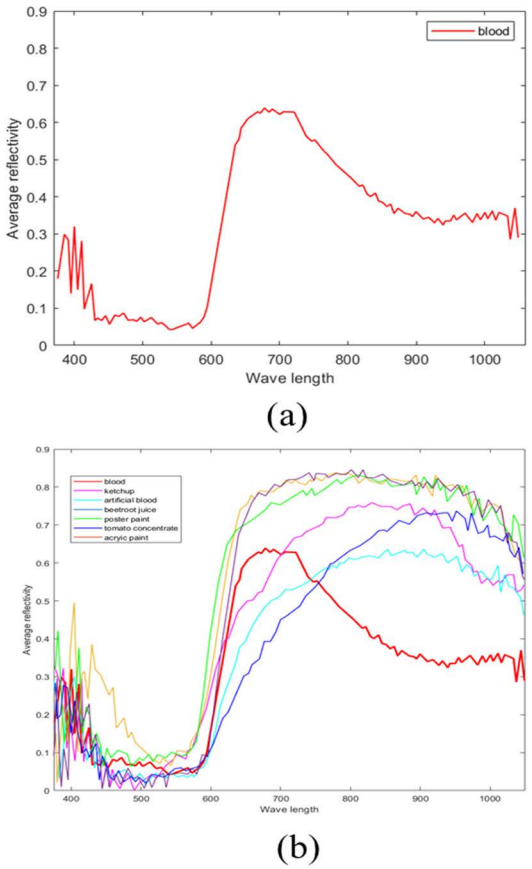

FIGURE 7. Average reflectance spectra of blood and six blood analogs: (a) blood; (b) seven liquids on a chart.

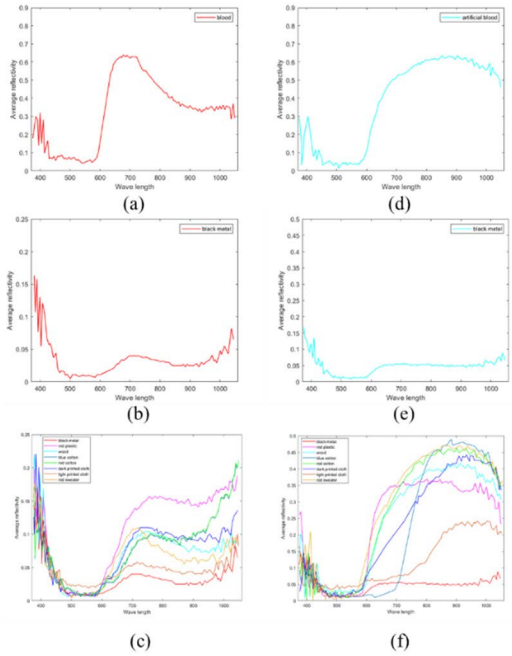

FIGURE 8. Average reflectance spectra of bloodstains and artificial bloodstains on different substrates: (a) standard bloodstain spectra; (b) bloodstains on black metal substrates; (c) bloodstains on eight different substrates; (d) standard artificial bloodstain spectra; (e) artificial bloodstains on black metal substrates; (f) artificial bloodstains on eight different substrates.

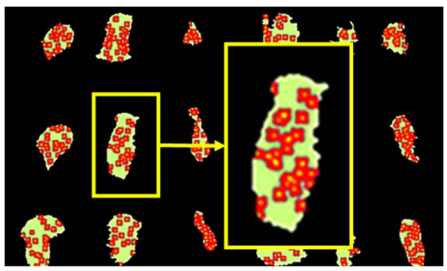

FIGURE 9. Selected training pixels and testing examples.

reflection amplitude value in the visible 600 nm band and beyond due to the red color of the bloodstain. The average reflection spectra of all pixels of the hyperspectral bloodstain and blood analog images under laboratory conditions are shown in Figure 7.

In more complex scenes, the spectrum curve of bloodstains varies greatly and is influenced by different substrates. As shown in Figure 8, it can be seen that different substrates affect the amplitude variation of the bloodstain spectral curve. This huge difference brings great difficulties to the intuitive classification of samples. Therefore, in complex scenes, it is necessary to complete the bloodstain hyperspectral data analysis work through deep learning.

C. CNN TRAINING PROCESS

Since 2D-CNN and 3D-CNN are based on pixels as input objects, a uniform training and test set needs to be created for each image. The aim is to avoid regions of non-empty intersections in the training and test sets. We select a set of samples with $n_{train} = 5\% \cdot ns$ in each class, and finally select the least number of pixels in the class as training pixels. The advantage of this is that each class is represented by the same number of samples. On the other hand, the neighborhoods of 2 pixels around the training pixels will be marked as unavailable. All the marked pixels will constitute a testing set and the result of this process is shown in Figure 9. Thus for each image, a different set of randomized training pixels is prepared. And use the same training set for each network to ensure comparability of results across architectures. Results are run for each scenario for the network type/image configuration using the fixed training dataset specified above.

To pursue a higher detection performance, we train the experimental scene and the complex scene separately, with a total of 36,548 sample inputs. Figure 10 shows the training process of the blood spectral data collected in the experimental scene in the proposed network model in this study. Figure 10(a) shows that the final loss functions of the training and testing sets are stable at 0.000352 and 0.002247 after 100 rounds of training. Figure 10(b) shows that the final classification accuracies of the training and

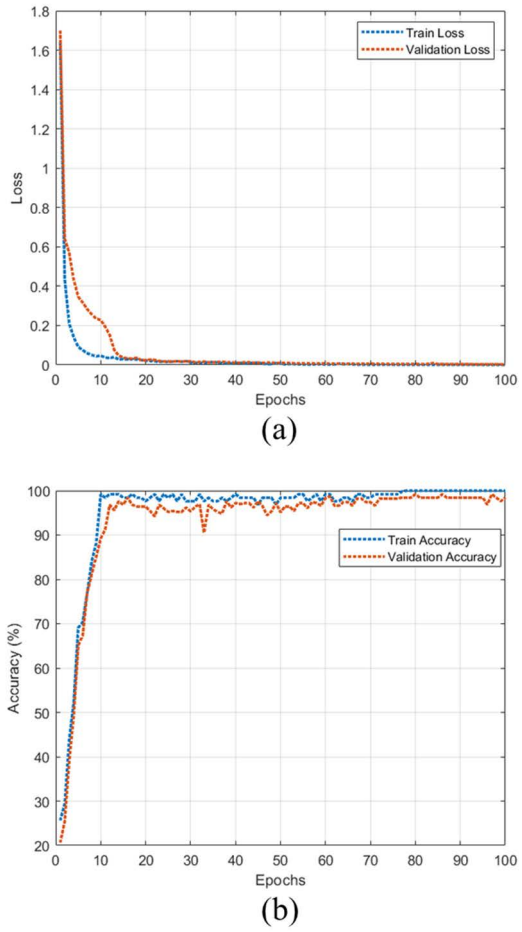

FIGURE 10. Bloodstain spectral data of laboratory scene by 2D-3D CNN training process: (a) Loss function; (b) Accuracy of classification.

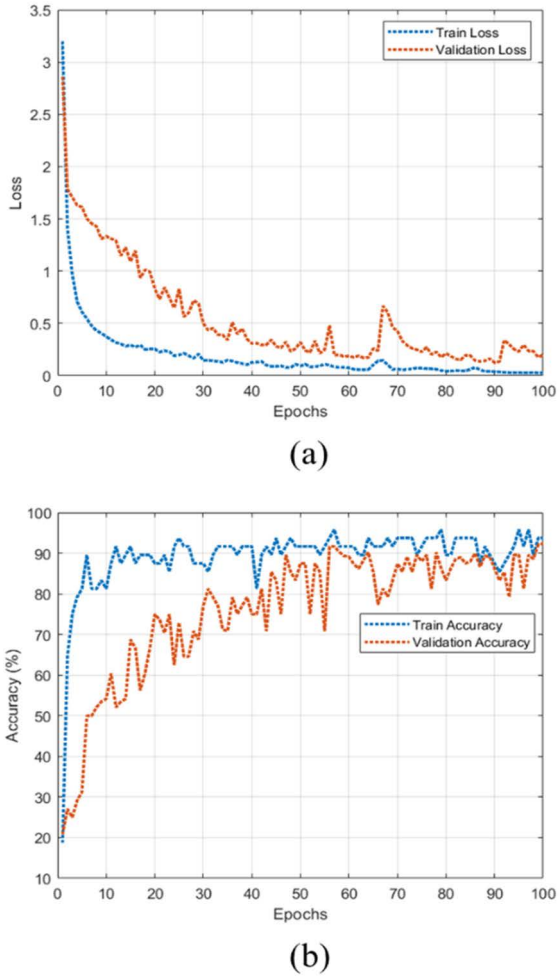

FIGURE 11. Bloodstain spectral data of complex scenes by 2D-3D CNN training process:(a) Loss function; (b) Accuracy of classification.

testing sets reach 100% and 98.41%, respectively, after 100 rounds of training.

Figure 11 shows the training process of the bloodstain spectral data collected in more complex scenes using the proposed network model in this study. Figure 11(a) shows that the final loss functions of the training and testing sets are stable at 0.026 and 0.02 after 100 rounds of training for the hyperspectral data, which indicates that the model has reached a stable optimal training state graph in a more complex scene. Figure 11(b) represents the final classification accuracies of 93.75% and 92.42% for the training set and testing set, respectively, after 100 rounds of training for hyperspectral data. Compared with the traditional methods, the model proposed in this study has obvious advantages and can identify bloodstains more accurately.

D. MODEL OBJECTIVE EVALUATION RESULTS

In this section, we use four models to train and test the same data input under experimental scenes and complex scenes, respectively, in order to ensure the objectivity of the model quality, and finally the results are compared. The models being compared are 1D-CNN, 2D-CNN, 3D-CNN and the proposed model in this study. Table 2 shows the

TABLE 2. Performance comparison of different models in standard experimental scenes.

Model	Bloodstain accuracy	Average accuracy	kappa
1D-CNN	99.8%	99.33%	0.991
2D-CNN	99.5%	99.52%	0.994
3D-CNN	99.8%	99.55%	0.994
Proposed	99.7%	99.77%	0.997

comparison results of the four models under the experimental scenes. From the data, it can be seen that the detection results of all four models are excellent in the experimental scene without much difference. It shows that the detection of bloodstains using hyperspectral techniques has better results in the standard experiment.

Table 3 shows the comparison results of the four models under complex scenes. From the results, it can be seen that under more complex scenes, the proposed model in this study achieves an accuracy of 95.4% for bloodstain recognition, an average accuracy of 95.39% for classification

TABLE 3. Performance comparison of different models in complex scenes.

Model	Bloodstain accuracy	Average accuracy	kappa
1D-CNN	49.9%	69.36%	0.630
2D-CNN	86.8%	79.77%	0.749
3D-CNN	88.1%	89.78%	0.873
Proposed	95.4%	95.39%	0.944

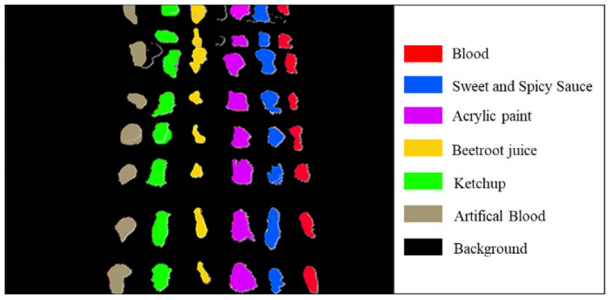

FIGURE 12. Hyperspectral image visualization.

TABLE 4. Training time and test time using 1D-CNN, 2D-CNN, 3D-CNN and the proposed method on data under laboratory conditions and complex scenes. Training time is in minutes (m) and testing time is in seconds (s).

Data	1D-CNN		2D-CNN		3D-CNN		Proposed	
	Train (m)	Test (s)	Train (m)	Test (s)	Train (m)	Test (s)	Train (m)	Test (s)
laboratory	1.5	5.1	1.6	3.5	16.5	4.3	9.4	3.8
complex	2.3	26.8	2.3	17.3	35.3	37.4	20.3	16.0

of bloodstains and bloodstain analogs, as well as a kappa coefficient of 0.944. Compared with other models, our proposed method in this study clearly has a huge advantage.

Hyperspectral images contain rich spectral and spatial information, which provides visualization possibilities to identify bloodstains and bloodstain analogs in complex scenes. The mixed 2D-3D CNN model is used for the identification and detection of bloodstains and bloodstain analogs, and mapped out to better understand the distribution of bloodstains and bloodstain analogs. Figure 12 shows the visualization of bloodstains and bloodstain analogs, and this visualization is consistent with the results of the analysis of the model in Table 2.

The computational efficiency of the proposed mixed 2D-3D CNN model in this study is presented in Table 4, in the form of training and testing time. This proposed model is more efficient than other models.

IV. CONCLUSION

In this study, bloodstain and blood analogs in different scenes are successfully detected and identified using visible/near-infrared hyperspectral combined with mixed 2D-3D CNN technology. The mixed CNN model for bloodstain identification is proposed to address the challenge that hyperspectral bloodstain detection is difficult to accomplish in complex scenes. Next, a large number of spectral data are analyzed by principal component and reduced dimension processing. Then, training and testing are carried out and the models are evaluated and compared. Finally, the distribution of bloodstain and blood analogs is visualized. The experimental results show that the model has a 95.4% accuracy in identifying bloodstain and bloodstain analogs on complex substrates, which has a state of the art than other detection methods. In this study, we use hyperspectral imaging technology for fast and non-destructive bloodstain detection and combined it with the mixed CNN model to improve the accuracy of bloodstain recognition. This detection method provides a certain reference value for other detection fields and online detection work. In future work, we will consider how to determine the exposure time and blood type of bloodstains by this technique.

REFERENCES

[1] S. Cadd, B. Li, P. Beveridge, W. T. O'Hare, A. Campbell, and M. Islam, "The non-contact detection and identification of blood stained fingerprints using visible wavelength reflectance hyperspectral imaging: Part 1," *Sci. Justice*, vol. 56, no. 3, pp. 181–190, May 2016, doi: 10.1016/j.scijus.2016.01.004.

[2] Y. Seo, G. Kim, J. Lim, A. Lee, B. Kim, J. Jang, C. Mo, and M. S. Kim, "Non-destructive detection pilot study of vegetable organic residues using VNIR hyperspectral imaging and deep learning techniques," *Sensors*, vol. 21, no. 9, p. 2899, Apr. 2021, doi: 10.3390/s21092899.

[3] M. Zhu, D. Huang, X. Hu, W. Tong, B. Han, J. Tian, and H. Luo, "Application of hyperspectral technology in detection of agricultural products and food: A review," *Food Sci. Nutrition*, vol. 8, no. 10, pp. 5206–5214, Oct. 2020, doi: 10.1002/fsn3.1852.

[4] H.-J. He and D.-W. Sun, "Hyperspectral imaging technology for rapid detection of various microbial contaminants in agricultural and food products," *Trends Food Sci. Technol.*, vol. 46, no. 1, pp. 99–109, Nov. 2015, doi: 10.1016/j.tifs.2015.08.001.

[5] S. R. Shinde, K. Bhavsar, S. Kimbahune, S. Khandelwal, A. Ghose, and A. Pal, "Detection of counterfeit medicines using hyperspectral sensing," in *Proc. 42nd Annu. Int. Conf. IEEE Eng. Med. Biol. Soc. (EMBC)*, Jul. 2020, pp. 6155–6158, doi: 10.1109/EMBC44109.2020.9176419.

[6] J. He, Y. He, and A. C. Zhang, "Determination and visualization of peimine and peiminine content in fritillaria thunbergii bulbi treated by sulfur fumigation using hyperspectral imaging with chemometrics," *Molecules*, vol. 22, no. 9, p. 1402, Aug. 2017, doi: 10.3390/molecules22091402.

[7] J. Marotz, A. Kulcke, F. Siemers, D. Cruz, A. Aljowder, D. Promny, G. Daeschlein, and T. Wild, "Extended perfusion parameter estimation from hyperspectral imaging data for bedside diagnostic in medicine," *Molecules*, vol. 24, no. 22, p. 4164, Nov. 2019, doi: 10.3390/molecules24224164.

[8] J. Marotz, A. Kulcke, F. Siemers, D. Cruz, and A. Aljowder, "Extended perfusion parameter estimation from hyperspectral imaging data for bedside diagnostic in medicine," *Molecules*, vol. 24, no. 22, p. 4164, 2019, doi: 10.3390/molecules24224164.

[9] Y. Hu, L. Xu, P. Huang, X. Luo, P. Wang, and Z. Kang, "Reliable identification of oolong tea species: Nondestructive testing classification based on fluorescence hyperspectral technology and machine learning," *Agriculture*, vol. 11, no. 11, p. 1106, Nov. 2021, doi: 10.3390/agriculture11111106.

[10] M. Sricharoonratana, A. K. Thompson, and S. Teerachaichayut, "Use of near infrared hyperspectral imaging as a nondestructive method of determining and classifying shelf life of cakes," *LWT*, vol. 136, Jan. 2021, Art. no. 110369, doi: 10.1016/j.lwt.2020.110369.

[11] K. Książek, M. Romaszewski, P. Głomb, B. Grabowski, and M. Cholewa, "Blood stain classification with hyperspectral imaging and deep neural networks," *Sensors*, vol. 20, no. 22, p. 6666, Nov. 2020, doi: 10.3390/s20226666.

[12] J. M. Bioucas-Dias, A. Plaza, G. Camps-Valls, P. Scheunders, N. Nasrabadi, and J. Chanussot, "Hyperspectral remote sensing data analysis and future challenges," *IEEE Geosci. Remote Sens. Mag.*, vol. 1, no. 2, pp. 6–36, Jun. 2013, doi: 10.1109/MGRS.2013.2244672.
[13] Y. Dong, B. Du, L. Zhang, and L. Zhang, "Dimensionality reduction and classification of hyperspectral images using ensemble discriminative local metric learning," *IEEE Trans. Geosci. Remote Sens.*, vol. 55, no. 5, pp. 2509–2524, May 2017, doi: 10.1109/TGRS.2016.2645703.
[14] Y. Tarabalka, M. Fauvel, J. Chanussot, and J. A. Benediktsson, "SVM- and MRF-based method for accurate classification of hyperspectral images," *IEEE Geosci. Remote Sens. Lett.*, vol. 7, no. 4, pp. 736–740, Oct. 2010, doi: 10.1109/LGRS.2010.2047711.
[15] S. Mei, J. Ji, J. Hou, X. Li, and Q. Du, "Learning sensor-specific spatial–spectral features of hyperspectral images via convolutional neural networks," *IEEE Trans. Geosci. Remote Sens.*, vol. 55, no. 8, pp. 4520–4533, Aug. 2017, doi: 10.1109/TGRS.2017.2693346.
[16] Y. Ding, X. Zhao, Z. Zhang, W. Cai, N. Yang, and Y. Zhan, "Semi-supervised locality preserving dense graph neural network with ARMA filters and context-aware learning for hyperspectral image classification," *IEEE Trans. Geosci. Remote Sens.*, vol. 60, pp. 1–12, 2022, doi: 10.1109/TGRS.2021.3100578.
[17] Y. Ding, X. Zhao, Z. Zhang, W. Cai, and N. Yang, "Graph sample and aggregate-attention network for hyperspectral image classification," *IEEE Geosci. Remote Sens. Lett.*, vol. 19, pp. 1–5, 2022, doi: 10.1109/LGRS.2021.3062944.
[18] Y. Ding, X. Zhao, Z. Zhang, W. Cai, and N. Yang, "Multiscale graph sample and aggregate network with context-aware learning for hyperspectral image classification," *IEEE J. Sel. Topics Appl. Earth Observ. Remote Sens.*, vol. 14, pp. 4561–4572, 2021, doi: 10.1109/JSTARS.2021.3074469.
[19] S. Huang, P. Wang, Y. Tian, P. Bai, D. Chen, C. Wang, J. Chen, Z. Liu, J. Zheng, W. Yao, J. Li, and J. Gao, "Blood species identification based on deep learning analysis of Raman spectra," *Biomed. Opt. Exp.*, vol. 10, no. 12, p. 6129, Dec. 2019, doi: 10.1364/boe.10.006129.
[20] J. Gao, L. Zhao, J. Li, L. Deng, J. Ni, and Z. Han, "Aflatoxin rapid detection based on hyperspectral with 1D-convolution neural network in the pixel level," *Food Chem.*, vol. 360, Oct. 2021, Art. no. 129968, doi: 10.1016/j.foodchem.2021.129968.
[21] H. Gao, S. Lin, Y. Yang, C. Li, and M. Yang, "Convolution neural network based on two-dimensional spectrum for hyperspectral image classification," *J. Sensors*, vol. 2018, pp. 1–13, Aug. 2018, doi: 10.1155/2018/8602103.
[22] S. Qiao, Q. Wang, J. Zhang, and Z. Pei, "Detection and classification of early decay on blueberry based on improved deep residual 3D convolutional neural network in hyperspectral images," *Scientific Program.*, vol. 2020, pp. 1–12, May 2020, doi: 10.1155/2020/8895875.
[23] P. Williams, P. Geladi, G. Fox, and M. Manley, "Maize kernel hardness classification by near infrared (NIR) hyperspectral imaging and multivariate data analysis," *Analytica Chim. Acta*, vol. 653, no. 2, pp. 121–130, Oct. 2009, doi: 10.1016/j.aca.2009.09.005.
[24] J. Hu, Y. Kuang, B. Liao, L. Cao, S. Dong, and P. Li, "A multichannel 2D convolutional neural network model for task-evoked fMRI data classification," *Comput. Intell. Neurosci.*, vol. 2019, pp. 1–9, Dec. 2019, doi: 10.1155/2019/5065214.
[25] J.-H. Kim and C. S. Won, "Action recognition in videos using pre-trained 2D convolutional neural networks," *IEEE Access*, vol. 8, pp. 60179–60188, 2020, doi: 10.1109/ACCESS.2020.2983427.

YUNAN HE is currently pursuing the master's degree with the School of Physics, Changchun University of Science and Technology, China. Her main research interests include non-destructive testing and control techniques, spectral analysis, and imaging processing.

CHENXUAN YANG is currently pursuing the master's degree with the School of Physics, Changchun University of Science and Technology, China. His main research interests include imaging processing, computer modeling, and optoelectronic imaging devices.

SHENG JIANG is currently working as an Associate Professor with the Changchun University of Science and Technology. He has published nearly 20 SCI and EI articles in several high-level journals and applied for two patents. His research interests include artificial intelligence and image processing, multisource information fusion, big data analysis, and other related fields.

ZHIJI DENG is currently a Researcher with Zhejiang Dahua Technology Company Ltd. His research interests include smart the IoT applications and big data analysis.

PENG ZHAO is currently an Associate Researcher with the Changchun University of Science and Technology. His research interests include infrared thermal imaging, optoelectronic imaging systems, and harmful gas detection systems.

YE LI was a Professor with the Changchun University of Science and Technology, where he is currently the Director of the School of Science, Institute of Optoelectronics Science, and the Optoelectronic Devices and Applied Technology Innovation Center. He has authored or coauthored 114 peer-reviewed academic journals. His main research interests include optoelectronic imaging devices and systems.